

Electronic supplementary Information

Interfacially stacked covalent porous polymer on graphene favors electronic mobility: Ensuring accelerated oxygen reduction reaction kinetics by in situ study

Greesh Kumar,^{†a} Sabuj Kanti Das,^{†a} Erakulan E. Siddharthan,^b Ashmita Biswas,^a Sakshi Bhardwaj^a, Manisha Das,^a Ranjit Thapa^b and Ramendra Sundar Dey^{a*}

^a*Institute of Nano Science and Technology, Sector-81, Mohali, 140306, Punjab, India.*

^b*Department of Physics, SRM University – AP, Amaravati 522240, Andhra Pradesh, India.*

**Corresponding author. E-mail: rsdey@inst.ac.in*

† These authors contributed equally to this work.

Section S1	Material, instrumentations and experimental part.
Fig. S1	¹ H NMR spectrum of PyTBE
Fig. S2	¹ H NMR spectrum of Br-Porphyrin
Fig. S3	¹ H NMR spectrum of FeP
Fig. S4	Synthesis of FePP via Suzuki C-C cross coupling reaction and further modification via exfoliation.
Fig. S5	N ₂ adsorption/desorption isotherm with Pore size distribution (inset) of FePP
Fig. S6	Full survey of XPS survey of FePP@G _{30/3/7} catalyst and N1s spectra
Fig. S7	Full survey of XPS and C1s , N1S and Fe2p XPS spectra of FePP
Fig. S8	The corresponding EXAFS fitting curves of the FePP@G _{30/3/7} catalyst at k space
Fig. S9	The corresponding EXAFS fitting curves of the FePP catalyst at k space
Fig. S10	Cyclic voltammetry (CV) analysis of FePP@G _{30/3/7} , FePP and Pt/C catalysts in the presence of Ar and O ₂ saturated 0.1 M KOH electrolyte solution.
Fig. S11	Linear sweep voltammetry polarization curve of FePP@G _{30/3/7} , FePP@G _{20/3/7} , FePP@G _{40/3/7} , FePP_XC72 and FePP_superP catalysts.
Fig. S12	Linear sweep voltammetry (LSV) polarization curves of FePP@G _{30/3/7} , FePP@G _{30/1.5/7} , FePP@G _{30/5/7} , FePP@G _{30/3/5} , and FePP@G _{30/3/10} , catalysts.
Fig. S13	Electrochemical surface area analysis of FePP@G _{30/3/7} and FePP
Fig. S14	Electrochemical impedance spectroscopy (EIS) analysis of FePP@G _{30/3/7} and FePP catalysts Nyquist plot and equivalent circuit.
Fig. S15	Linear sweep voltammetry (LSV) polarization curve of FePP@G _{30/3/7} catalyst at all rotation speeds 625 to 4900 rpm in O ₂ saturated 0.1 M KOH electrolyte solution.
Fig. S16	Linear sweep voltammetry (LSV) polarization curve of FePP@G _{30/3/7} catalyst at 1600 rpm in O ₂ saturated 0.1 M KOH electrolyte solution with disk and ring current.
Fig. S17	K-L plots of FePP@G _{30/3/7} catalyst at different potential
Fig. S18	Linear sweep voltammetry (LSV) polarization curve of FePP catalyst all rotations from 625 to 4900 rpm, K-L Plots of FePP and No. of electrons and H ₂ O ₂ (%) of FePP catalyst in O ₂ saturated 0.1 M KOH electrolyte solution.
Fig. S19	XPS spectra of of FePP@G _{30/3/7} catalyst after stability (a) Full survey XPS spectra. High resolution deconvoluted (b) C1s (c) N1s and (d) Fe2p XPS spectra of FePP@G _{30/3/7} catalyst after stability.
Fig. S20	XPS spectra of of FePP catalyst after stability (a) Full survey XPS spectra. High resolution deconvoluted (b) C1s (c) N1s and (d) Fe2p XPS spectra of

	FePP catalyst after stability.
Fig. S21	Methanol-cross over durability (i-t) curve in presence of methanol in O ₂ -saturated 0.1 M KOH solution.
Fig. S22	CV analysis <i>FePP@G_{30/3/7}</i> catalyst with 1M CH ₃ OH and without CH ₃ OH in O ₂ saturated KOH electrolyte.
Fig. S23	CV analysis of Pt/C catalyst with 1M CH ₃ OH and without CH ₃ OH in O ₂ saturated KOH
Fig. S24	Schematic for in-situ Raman setup during ORR analysis performed in 0.1 M KOH solution
Fig. S25	In-situ FTIR spectra in argon media
Section S3	DFT Calculations
Fig. S26	Structure models of intermediates adsorbed on the surfaces.
Fig. S27	Projected density of states (PDOS) of the d-orbital of (a) FePP and (b) FePP between fixed graphene sheet and flake. Dashed vertical line represents Fermi level (E _F) and solid vertical line represents d-band center position.
Table T1	Raman spectroscopy analysis of all synthesized of FePP and FePP@G _{30/3/7} and EG catalysts
Table T2	Elemental analysis of FePP@G _{30/3/7} and FePP catalyst obtained from XPS analysis before and after stability.
Table T3	Different parameters obtained from the EXAFS fitting of FePP and FePP@G _{30/3/7} catalysts
Table T4	Electrochemical parameters of all the synthesized catalysts and Pt/C
Table T5	All the optimized exfoliated catalysts performances on the basis of electrocatalytic parameters
Table T6	Comparative literature survey with all electrochemical parameters
Table T7	Comparative summary of all the electronic as well as electrochemical parameters of FePP@G _{30/3/7} and FePP catalysts

Section-1

1. EXPERIMENTAL

1.1 Chemicals

Pyrrole (98%), Pyrene (98%), [1,1' Bis(diphenylphosphino)ferrocene]dichloropalladium(II), and Pd(PPh₃)₄ (99%) were purchase from Sigma-Aldrich. Bis(pinacolato)diboron (98%) and p-Bromobenzaldehyde (98%), were achieved from Spectrochem, India. All Solvents, FeCl₂, acid and base were bought from Merck, India. All chemicals were used without any further purification. 1,3,6,8-tetrakis(4,4,5,5-tetramethyl-1,3,2-dioxaborolan-2-yl) pyrene and 5,10,15,20-(tetra-4-bromophenyl) porphyrin Iron (II) were synthesized following the literature.

1.2 Synthesis of 1,3,6,8-tetrakis(4,4,5,5-tetramethyl-1,3,2-dioxaborolan-2-yl)pyrene (PyTBE):

A schlenk tube was charged with bis (pinacolato) diboron (4.4 g, 17.35 mmol), 1.5 g 1,3,6,8-tetrabromopyrene (2.9 mmol), Pd(dppf)Cl₂ (0.175 g, 0.25 mmol) and potassium acetate (1.75 g, 17.85 mmol) in 15 ml anhydrous DMSO solvent. The above mixture was backfilled with N₂ three times and heated the reaction mixture at 90 °C for 48 h under stirring condition. The reaction mixture was cooled to room temperature and extracted with Dichloromethane (DCM). The crude product was isolated by solvent evaporation and yellow color solid product obtained. The flash column chromatography was used for purification of crude yellow solid material on silica gel (60-120 mesh) using toluene /dichloromethane as an eluent. The tetra borylated product was isolated as grey solid (1.5 g, yield 76 %).¹

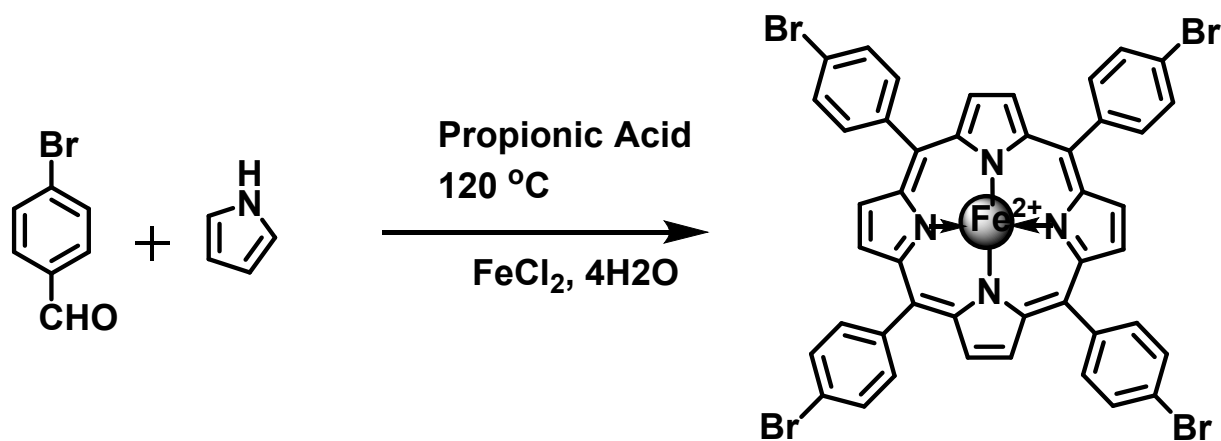
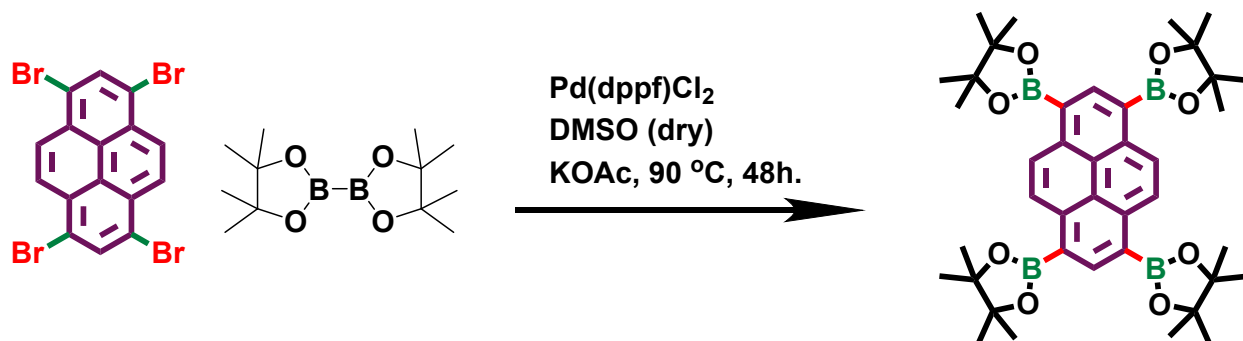
NMR: ¹H NMR (400 MHz, CDCl₃, ppm) 9.15 (s, 4H); 8.98 (s, 2H); 1.54 (s, 24H); 1.50 (s, 24H).

1.3 Synthesis of Br-Porphyrin and FeP-monomer

A mixture of p-bromobenzaldehyde (0.93 g, 5 mmol) in propionic acid (20 mL) was heated up to 120 °C and after that freshly prepared distilled pyrrole (0.35 mL, 5 mmol) was added to the solution and stirred for 4h at 120 °C and cooled to room temperature for 3 days. The blackish violet precipitate was collected through filtration and mixture was washed with plenty of methanol. The recrystallization of crude mixture was done from chloroform/methanol mixture to

get the pure product as a needle shape violet crystal (30% yield). The metalation step had been done by the mixing of $\text{FeCl}_2 \cdot 4\text{H}_2\text{O}$ (1500 mg, 7.54 mmol) and 5,10,15,20- Tetrakis(4'-bromobiphenyl) porphine (395 mg, 0.32 mmol) into a dried 250 mL flask in dry DMF (100 mL) under an argon atmosphere. Thereafter, the mixture was stirred at 120 °C overnight, cooled to room temperature, and aqueous HCl solution (3.0 M, 20 mL) was add by dropwise method. The precipitated mixture was filtered and washed with 3.0 M HCl and DI water. The product was further purified by recrystallization from chloroform and methanol twice to give FeP-monomer in 85 % yield. Both Br-porphyrin and FeP-monomer was characterized by using $^1\text{H-NMR}$. The peak (a) appeared at negative region (-2.9 ppm) in Br-porphyrin (Fig. S2), but it disappeared after metallation (Fig. S3). It is confirmed from this, Fe successfully coordinated with porphyrin moiety.

Synthesis of PyTBE ester and Fe-Porphyrin (FeP)



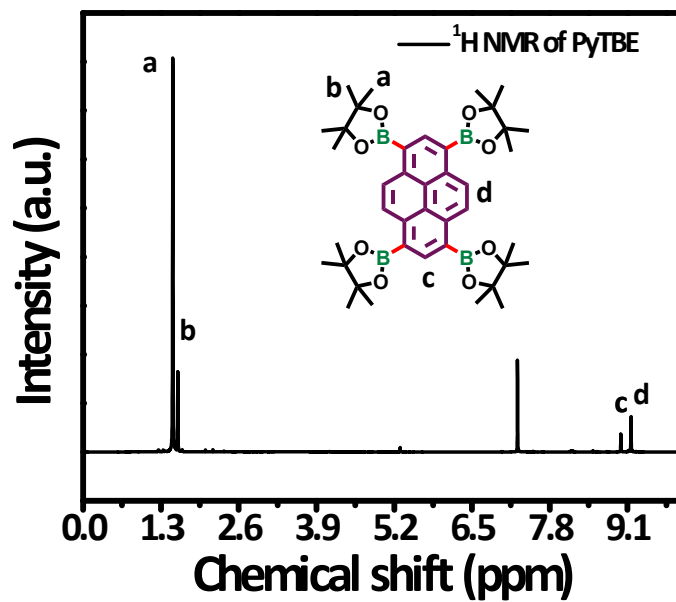


Fig. S1. ^1H NMR spectrum of PyTBE

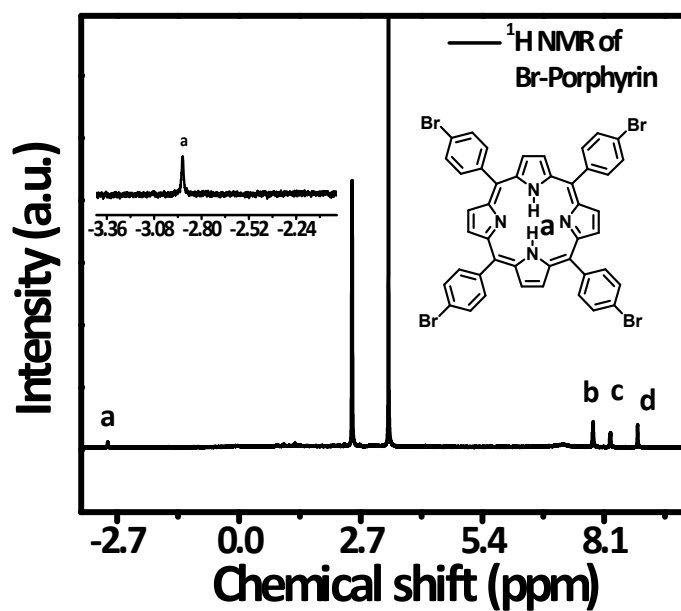


Fig. S2. ^1H NMR spectrum of Br-Porphyrin

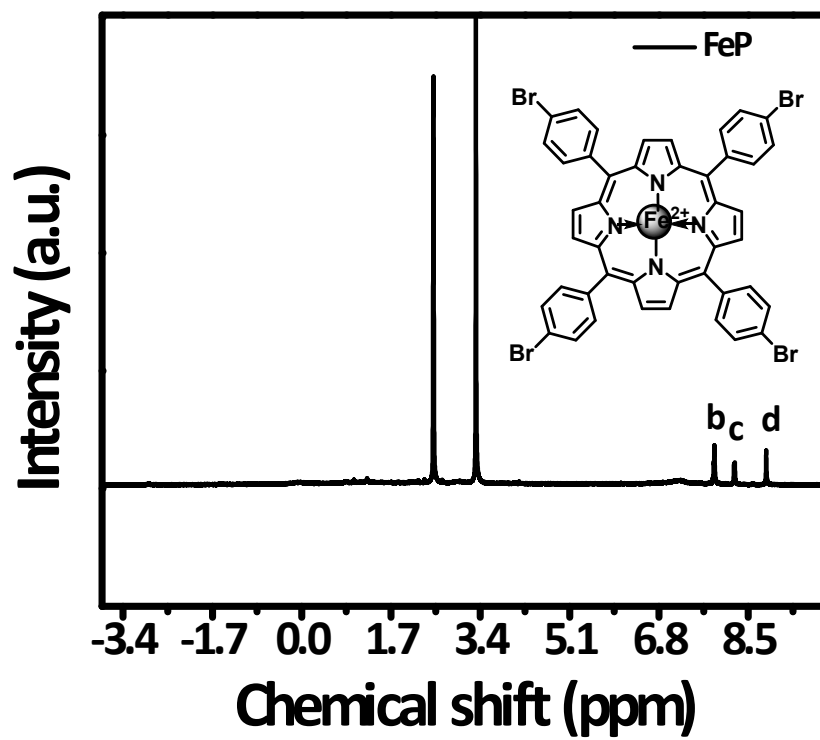


Fig. S3. ^1H NMR spectrum of FeP.

1.3 Synthesis of FePP

For the synthesis of FePP, 424 mg of 1,3,6,8-tetrakis(4,4,5,5-tetramethyl-1,3,2-dioxaborolan-2-yl)pyrene (0.4 mmol) was taken along with 608 mg 5,10,15,20-(tetra-4-bromophenyl)porphyrin Fe (II) complex (0.4 mmol) in a Schlenk tube. After that, 24 mL of 1,4-dioxane and 6 mL of 3 (M) aqueous K_2CO_3 solution was added, followed by the final addition of 100 mg of $Pd(PPh_3)_4$. The total mixture was put under the process of degassing and was backfilled four times with N_2 by Freeze-Pump-Thaw method. The mixture was finally heated in an oil bath at $100^\circ C$ along with continuous stirring for 2 days. In the final step, the mixture was allowed to cool and then once it came to room temperature it was diluted with water-methanol mixture, followed by consequent filtration and washing several times with distilled water and THF. The solvent extraction of the final precipitate was carried out with MeOH:THF (1:1) for another 48 hours by the Soxhlet apparatus to achieve Pd and monomers free material and dry under vacuum at $100^\circ C$. The isolated yield was 75%.

1.4 Synthesis of FePP@G_{30/3/7} and other electrocatalysts

Synthesis of FePP@G_{30/3/7} was carried out by electrochemical exfoliation technique using graphene sheet of $1*2\text{ cm}^2$ as cathode and anode into a dispersed solution of FePP in 1.5 M H_2SO_4 . The exfoliation has been done with 30 mg of FePP in 20 mL acidic solution at 3V for 7 min followed by the sonication at 30 min. After that, the precipitate was washed several times with DI water until the solution became neutral. Finally the material FePP@G_{30/3/7} as represented was obtained by washing with DI water and ethanol and collected through centrifuges under 10000 rpm and dry under vacuum at $100^\circ C$. Similarly the exfoliation has also been done with different amount of FePP (20 mg, 30 mg and 40 mg) in 20 ml acidic solution at different applied potentials (1.5V, 3V and 5V) for different time (5 min, 7 min, and 10 min) followed by the sonication at 30 min and materials represented as FePP@G_{30/1.5/7}, FePP@G_{30/5/7}, FePP@G_{30/3/5}, FePP@G_{30/3/10}, FePP@G_{20/3/7}, FePP@G_{40/3/7}, catalysts. The synthesis of FePP/G was synthesized by using exfoliated graphene in 20 mL 1.5 M H_2SO_4 solution, which was exfoliated at 3 V for 7 minutes and 30 mg of FePP mixed. The solution was stirred for 3 hours. The solution was washed with water and ethanol and collected through centrifuged under 10000 rpm and dry under vacuum at $100^\circ C$.

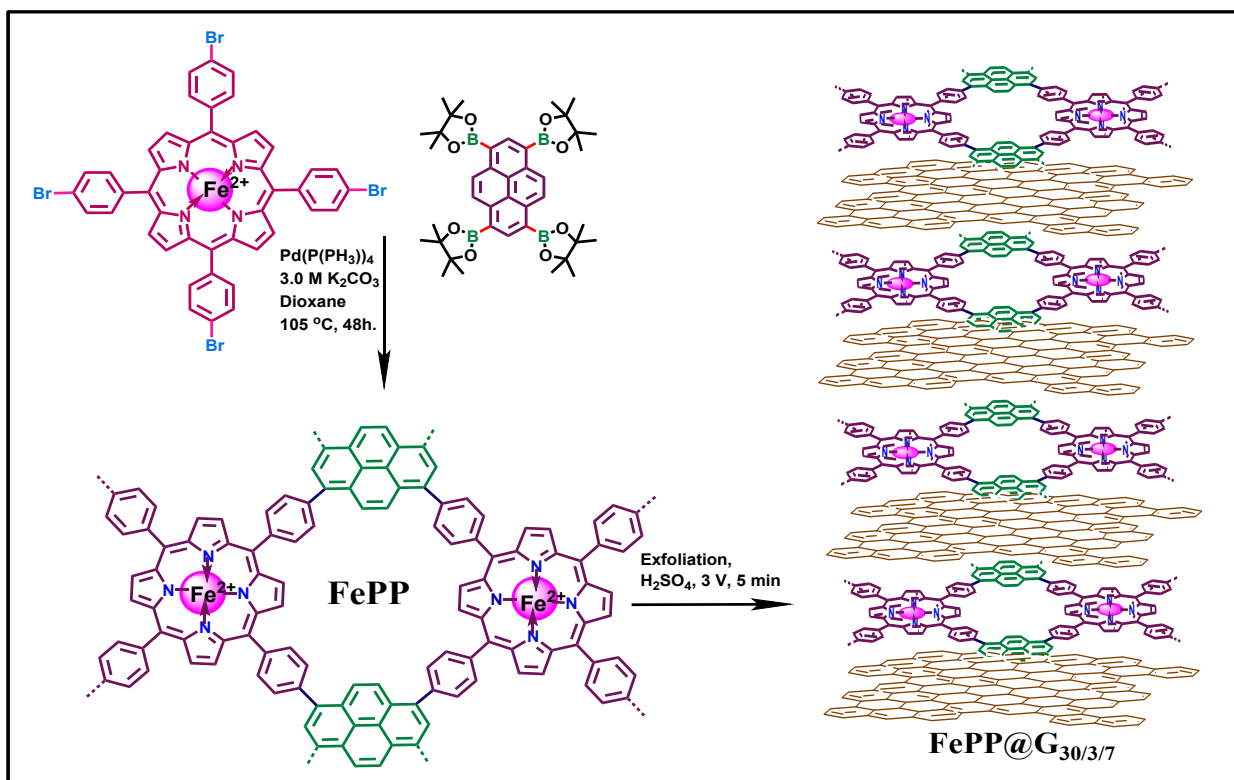


Fig. S4. Synthesis of FePP via Suzuki C-C cross coupling reaction and further modification via exfoliation.

1.5 Catalyst Characterization Technique.

X-Ray diffraction patterns of the powder samples were recorded with Bruker D8 advance X-ray diffractometer using (Cu K_{α} $\lambda=0.15406$ nm) to go through the crystalline nature of the as prepared material. Raman Spectroscopy was performed on a WITEC Focus Innovations Alpha-300 Raman confocal microscope at a laser wavelength of 532 nm. The compounds were dissolved in commonly used NMR solvents for liquid state proton and ^{13}C NMR and the corresponding data was recorded in Bruker DPX-400/500 NMR spectrometer. A 400MHz Bruker Advance II spectrometer was used at a mass frequency of 8 kHz to obtain the solid state ^{13}C CP-MAS NMR of the synthesized material. To determine the bond connectivity, FT-IR spectrum analysis was carried out by a PerkinElmer Spectrum 100 instrument. The visual morphological study and Energy dispersive X-ray spectroscopy for elemental analysis of the synthesized FePP and FePP@G₃₀ materials were done by Hitachi S-5200 instrument for field-emission scanning electron microscopy. Brunauer-Emmett-Teller (BET) study was carried out in Quantachrome Autosorb iQ by experimental volumetric adsorption/desorption of Nitrogen at 77 K to find the surface area of the material where the sample was processed for 6h degassing at 120 °C in vacuum and NLDFT or Non local density functional theory was used to calculate the pore size distribution. Solid state UV-Visible spectroscopy was carried out using Shimadzu UV-2401PC spectrophotometer. Solid-state photoluminescence (ss-PL) was carried out using RF-6000 spectro Fluorophotometer. X-ray photoelectron spectroscopy (XPS) analysis was carried out at 20 mA and 15 kV using an Omicron nanotech.

The Extended X-ray absorption fine structure spectrum (EXAFS) was performed at the Raja Ramanna Centre for Advanced Technology (RRCAT), Indore, India with the dispersive EXAFS beam line (BL-9) at Indus-2 synchrotron radiation source. The beam source was operated at 2.5 GeV (300 mA). A bent crystal Si (111) polychromator was used to select a band of energy in this beamline, the data for this study was collected in transmission mode for Fe foil, Fe₂O₃, FePP and FePP@G_{30/3/7} catalysts. All the spectra of the materials were measured under ambient condition. Data analysis of these materials was carried out using DEMETER programs. Athena and Artemis codes were utilized to extract the measured data and fit the profiles. The whole information about the atomic environments around central absorbing Fe atom, the nearest neighbour distances (R), mean deviation of distances (σ) as of the absorbing atoms and coordination numbers (N), were obtained from the Fourier transform $|\chi(R)|$ of the EXAFS oscillation curves.

CHI 760E electrochemical workstation, BioLogic VSP potentiostats and Metrohm multichannel Autolab (M204) electrochemical workstation were used to check the electrochemical activity of catalysts by using three electrode systems. For the experimental set up, a rotating disk electrode (RDE), rotating ring disk electrode (RRDE) and glassy carbon (GC) were used as the working electrode along with graphite rode (3mm diameter) and Ag/AgCl (3 M

KCl) electrode as counter and reference electrodes respectively. Our prepared material was drop casted on a pre-cleaned RDE/RRDE/GC electrodes by using 1, 0.3 and 0.05 μm alumina powder so that it can be used as the working electrode. To prepare the catalytic ink, 3 mg of material was dispersed in 1 mL, 1:1 isopropanol and DI water and it was sonicated for 30 min. The electrochemical activity of FePP@G_{30/3/7} and other catalysts were measured using Auto-lab by employing (CV), (LSV) Chronoamperometry Technique (CA) and (EIS) techniques using O₂-saturated 0.1 M KOH as electrolyte solution at room temperature.

1.6 Computational details:

All the calculations are performed in the Vienna Ab-initio Simulation Package (VASP) using non-spin polarized density functional theory.² Projected Augmented Wave (PAW) method is used to describe the potentials of the atoms³ with Generalized Gradient Approximation (GGA) is considered for exchange and correlation effects at Perdew-Burke-Ernzerhof (PBE) level.⁴ Plane wave cut-off energy of 450 eV is used for the calculations. Gamma centered 3x3x1 K-point grid is used for the brillouin zone sampling. Structural optimizations were done until the total energy converged less than 10⁻⁵ eV per atom and the maximum force converged less than 0.01 eV/Å. Grimme's DFT-D2 method was taken for Van der Waals dispersion correction.⁵ Henkelman's bader charge analysis is used for estimating the charges on the atoms.⁶ Fe-Porphyrin-Pyrene (FePP) moiety is modelled with the ends of the carbon atoms terminated with hydrogen atoms. 9x9 graphene supercell and graphene flake with 10 hexagonal rings are taken as substrate for FePP. To avoid any periodic interaction along the z-axis, vacuum of ~15Å is taken.

Section-2

Physical and electrochemical characterization

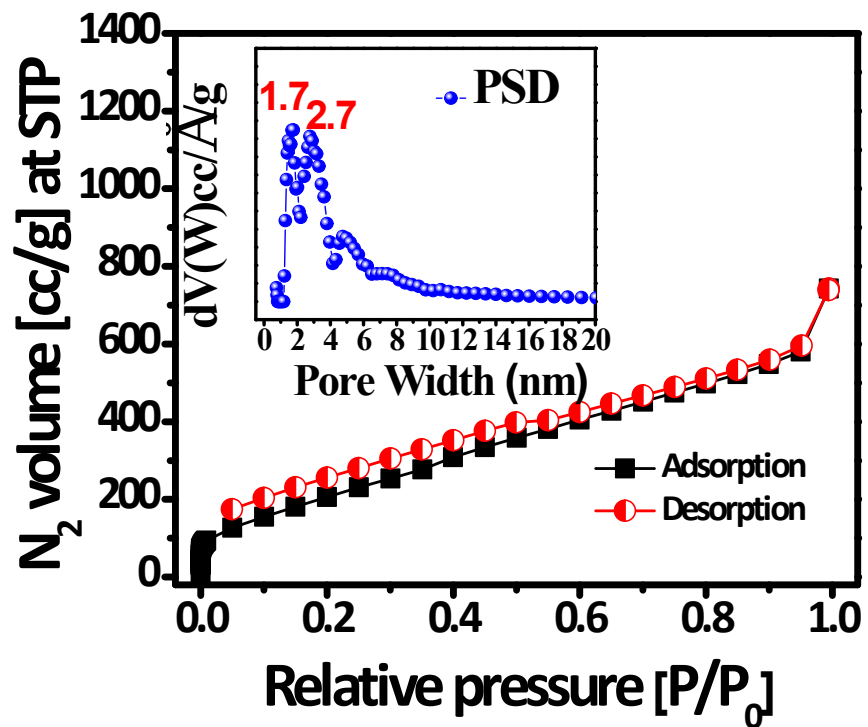


Fig. S5. N₂ adsorption/desorption isotherm with Pore size distribution (inset) of FePP.

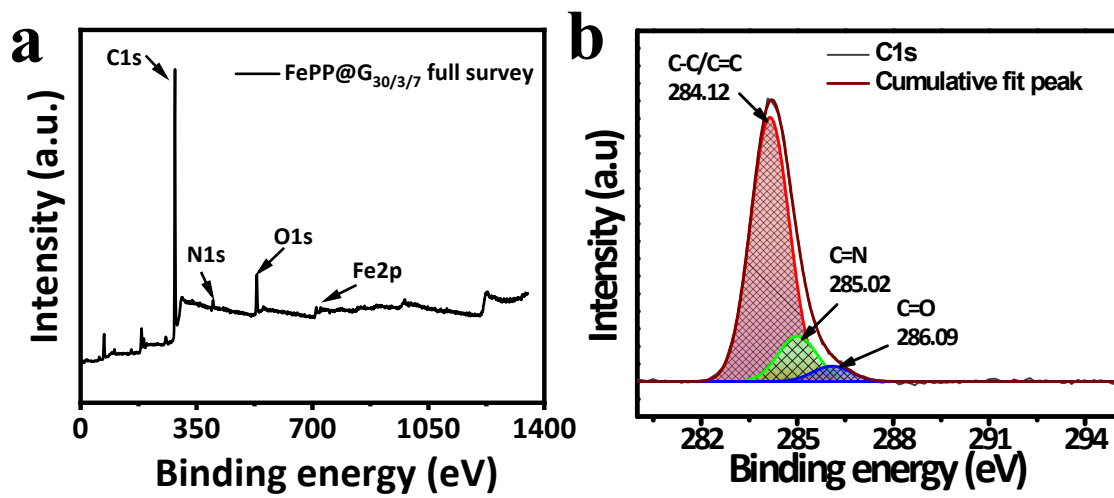


Fig. S6. (a) Full survey of XPS analysis of FePP@G_{30/3/7} catalyst (b) High resolution deconvoluted N1s XPS spectra.

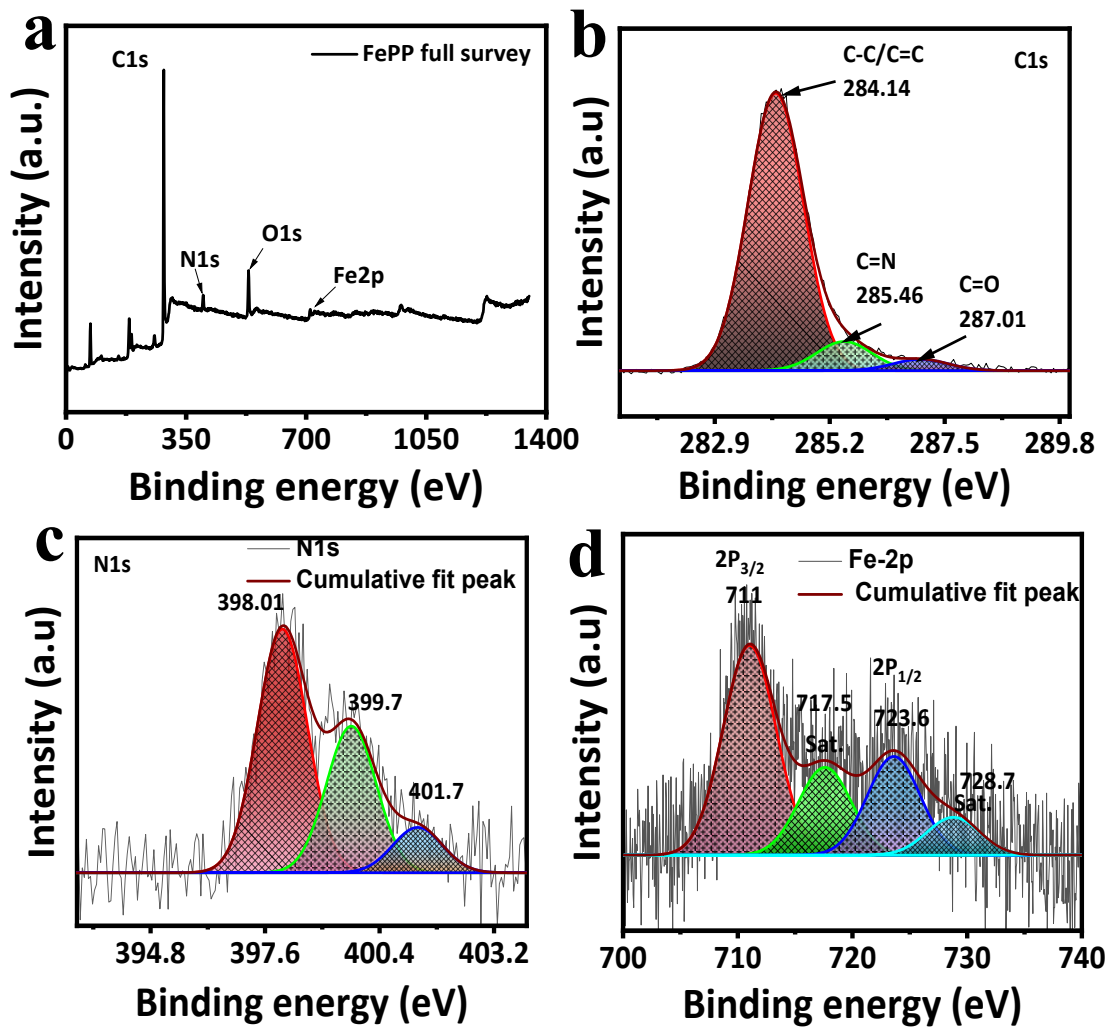


Fig. S7. XPS analysis of FePP catalyst (a) Full survey of XPS (b) C1s (c) N1s and (d) Fe2p XPS spectra.

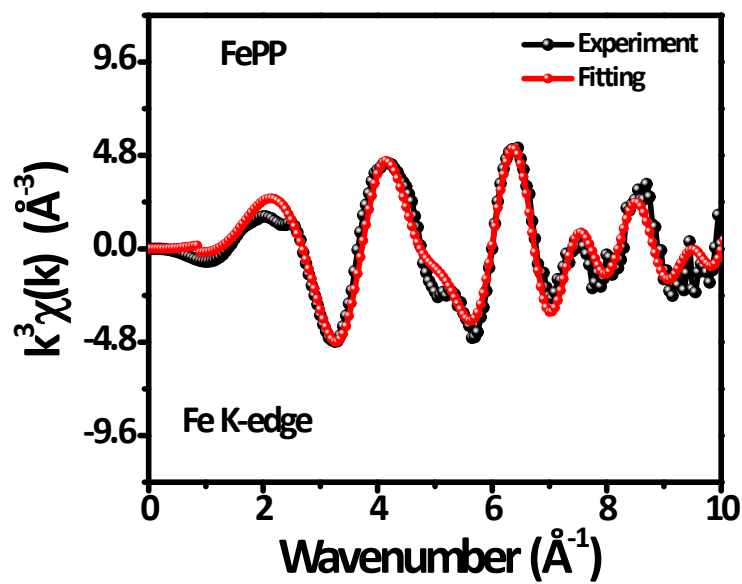


Fig. S8. The corresponding EXAFS fitting curves of the FePP catalyst at k space.

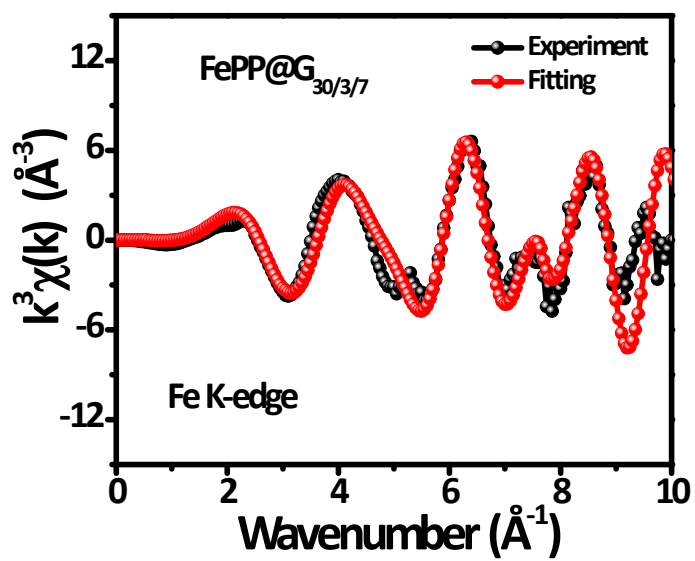


Fig. S9. The corresponding EXAFS fitting curves of the FePP@G_{30/3/7} catalyst at k space.

Formula used for conversion to standard electrode potential:

All the experiments were performed in Ag/AgCl (3 M KCl) reference electrode and potentials were converted to standard RHE (reversible hydrogen electrode) potential using (Equation 1) as reported in this manuscript. For 0.1 M KOH (pH>13) following equation was considered⁷:

$$E_{\text{RHE}} (\text{V}) = E_{\text{Ag/AgCl (3 M KCl)}} (\text{in V}) + (0.059 \times \text{pH}) + 0.210 \text{ V} \quad \text{Eq. (1)}$$

The calculation of electron transferred number (n) for ORR:

The number of electron transfer per O₂ participate in oxygen reduction reaction can be determined by Koutechy-Levich (K-L) equation:

$$\frac{1}{J} = \frac{1}{J_L} + \frac{1}{JK} = \frac{1}{B\omega^2} + \frac{1}{JK} \quad \text{Eq. (2)}$$

$$B = 0.62nFC_0 D_0^{2/3} \nu^{-1/6} \quad \text{Eq. (3)}$$

$$JK = nFkC_0 \quad \text{Eq. (4)}$$

J is the measured current density, J_L and J_K are the diffusion-limiting and kinetic current densities, ω is the angular velocity of the disk ($\omega = 2\pi N$, N is the linear rotation speed), F is the Faraday constant ($F = 96485 \text{ C mol}^{-1}$), n is the overall number of electrons transferred in oxygen reduction reaction, ν is the kinematic viscosity of the electrolyte, C_0 is the bulk concentration of O₂, k is the electron transfer rate constant, and D_0 is the diffusion coefficient of O₂ in electrolyte solution. The J_K value and B can be determined from the Koutechy-Levich (K-L) plots based on the Levich equation.

Rotating Ring-Disk Electrodes (RRDE) measurements were performed to calculate the undesirable intermediate hydrogen peroxide (%H₂O₂) and number of transfer electrons (n) which were determined by the following equations:

$$n = 4 \times \frac{I_D}{I_D + \frac{I_R}{N}} \quad \text{Eq. (5)}$$

$$\%H_2O_2 = 200 \times \frac{\frac{I_R}{N}}{\frac{I_R}{N} + I_D} \quad \text{Eq. (6)}$$

Where I_R is ring current, I_D is disk current and N is current collection efficiency of the Pt ring. N was determined to be 0.249 in this study.

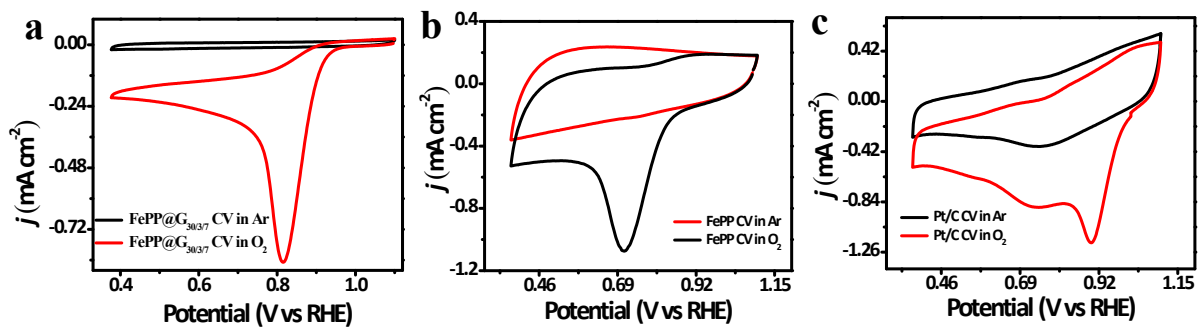


Fig. S10. Cyclic voltammetry (CV) analysis of (a) FePP@G_{30/37}, (b) FePP and (c) Pt/C catalysts in the presence of Ar and O₂ saturated 0.1 M KOH electrolyte solution.

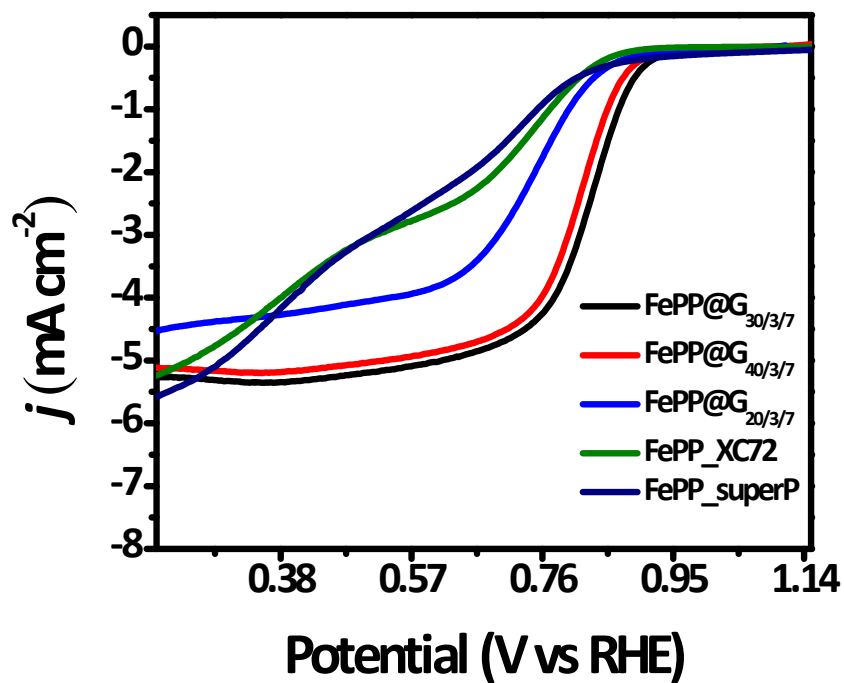


Fig. S11. Linear sweep voltammetry (LSV) polarization curves of FePP@G_{30/3/7}, FePP@G_{20/3/7}, FePP@G_{40/3/7}, FePP_XC72 and FePP_superP catalysts at 1600 rpm in O₂ saturated 0.1 M KOH electrolyte solution.

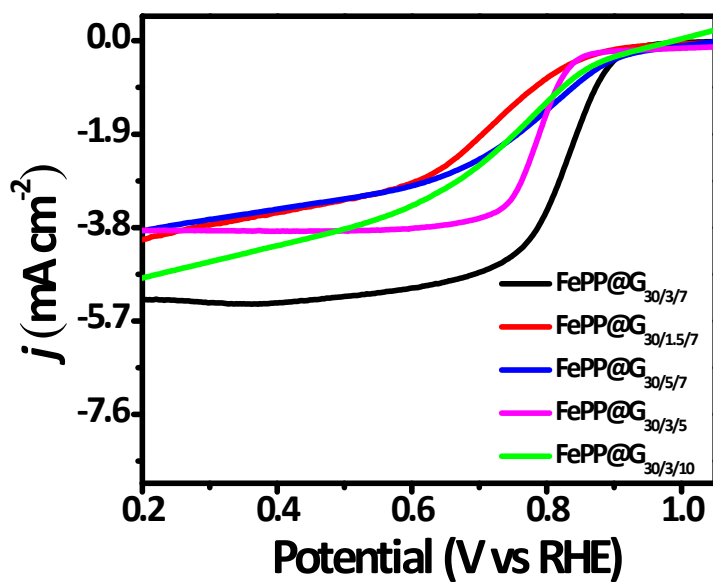


Fig. S12. Linear sweep voltammetry (LSV) polarization curves of FePP@G_{30/3/7}, FePP@G_{30/1.5/7}, FePP@G_{30/5/7}, FePP@G_{30/3/5}, and FePP@G_{30/3/10}, catalysts at 1600 rpm in O₂ saturated 0.1 M KOH electrolyte solution.

Electrochemical active surface area analysis:

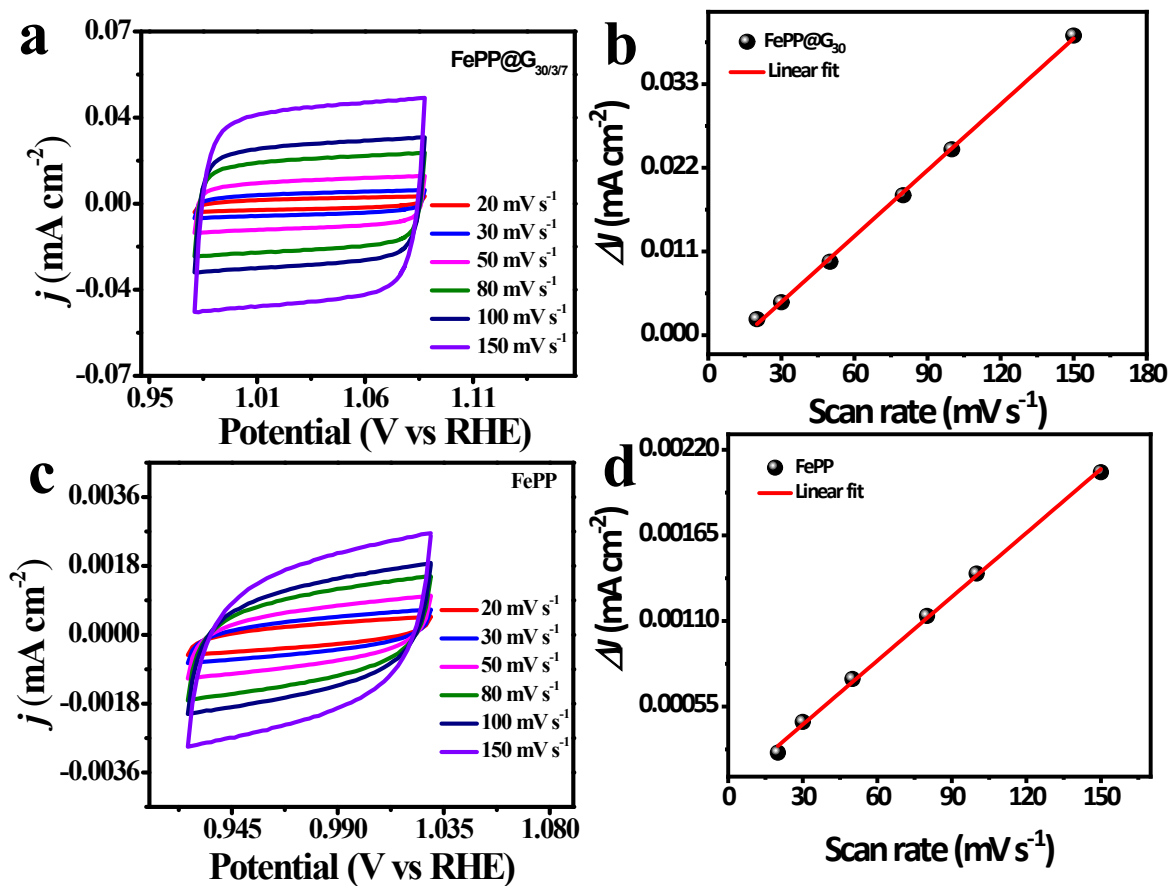


Fig. S13. Electrochemical active surface area analysis (a) CV curves of FePP@G_{30/37} at different scan rate (b) Linear fitting of capacitive currents of the FePP@G_{30/37} electrocatalyst vs scan rate (c) CV curves of FePP at different scan rate (d) Linear fitting of capacitive currents of the FePP electrocatalyst vs scan rate.

The electrochemical surface area analysis of FePP and FePP@G₃₀ have been done by using cyclic voltammetry curve which were taken at different scan rates from 20 mV s⁻¹ to 150 mV s⁻¹. The CV curves in a non-faradaic region were plotted as a function of various scan rates (20, 30, 50, 80, 100, 150 mV s⁻¹). Double layer capacitance (C_{dl}) calculated from the slope of the linear regression between the current density differences in the middle of the potential window of CV curves vs the scan rates. The ECSA was calculated by using following equation which is give below.

$$ECSA = \frac{C_{dl}}{C_s} \quad Eq. (7)$$

Where, C_s is the capacitance of the smooth electrode surface.

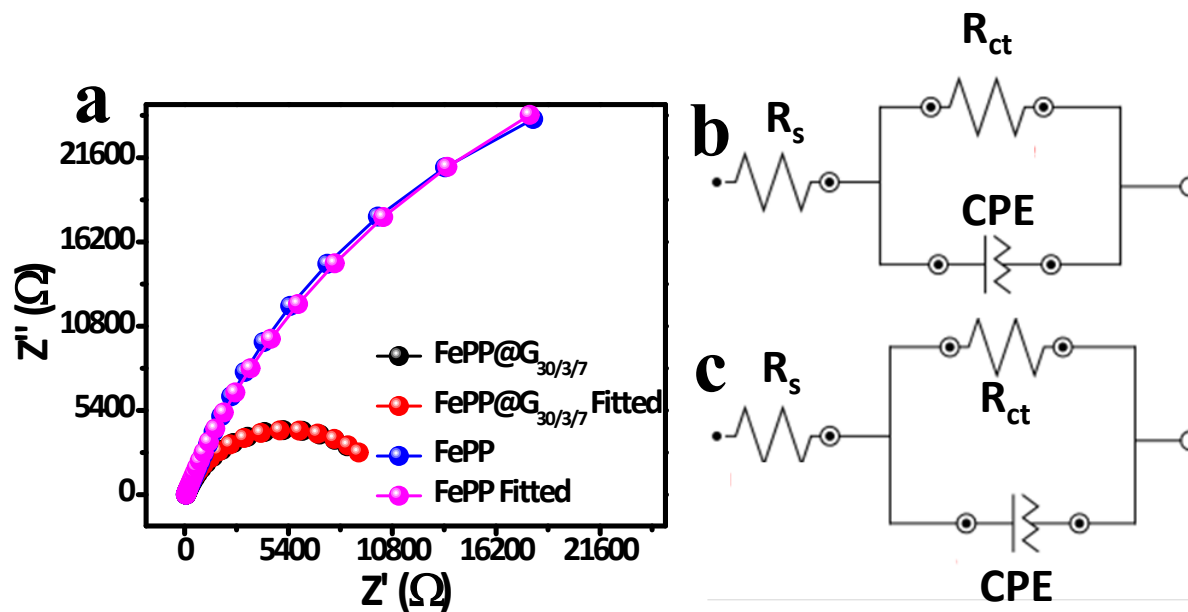


Fig. S14. (a) Electrochemical impedance spectroscopy (EIS) spectra of FePP@G_{30/3/7} and FePP and (b) equivalent circuit of FePP@G_{30/3/7} and (c) equivalent circuit of FePP.

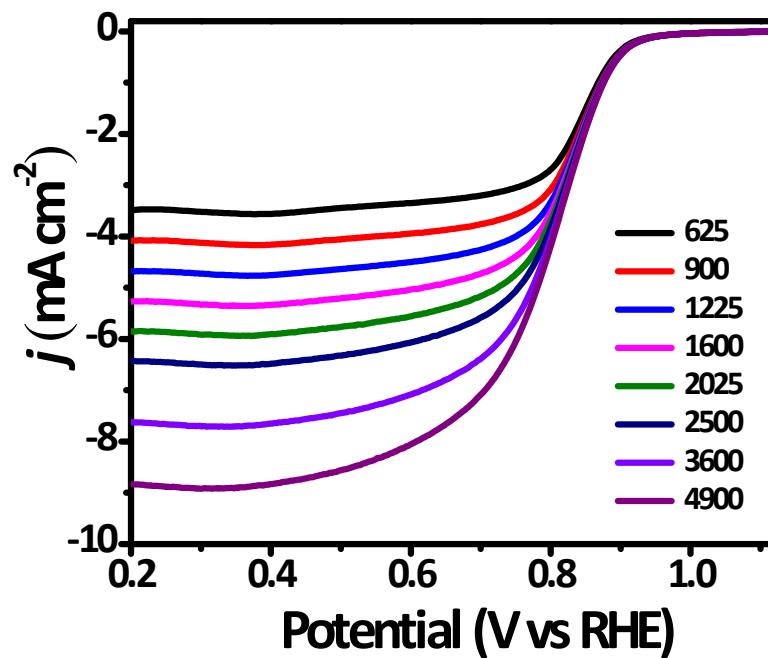


Fig. S15. Linear sweep voltammetry (LSV) polarization curve of FePP@G_{30/3/7} catalyst at all rotation speeds 625 to 4900 rpm in O₂ saturated 0.1 M KOH electrolyte solution.

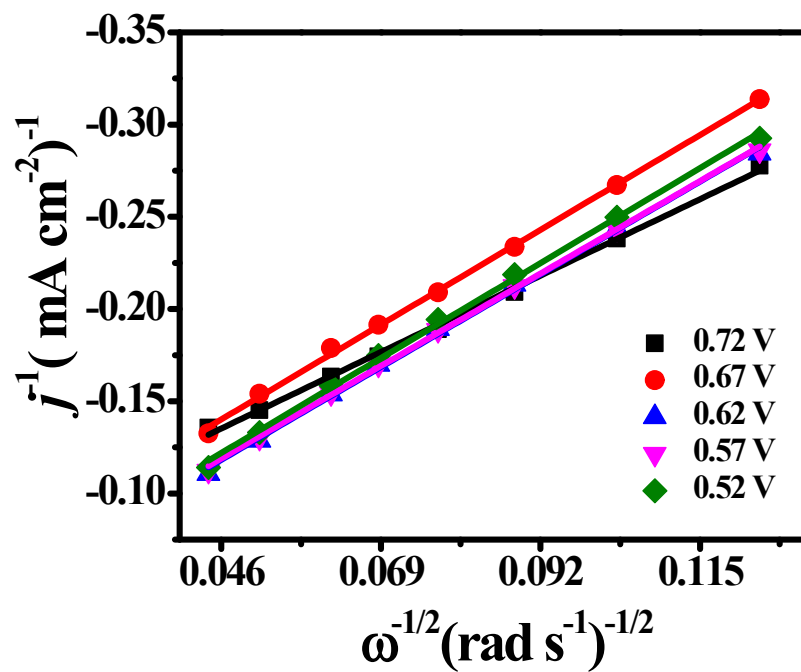


Fig. S16. K-L plots of FePP@G_{30/3/7} catalyst in O₂ saturated 0.1 M KOH electrolyte solution.

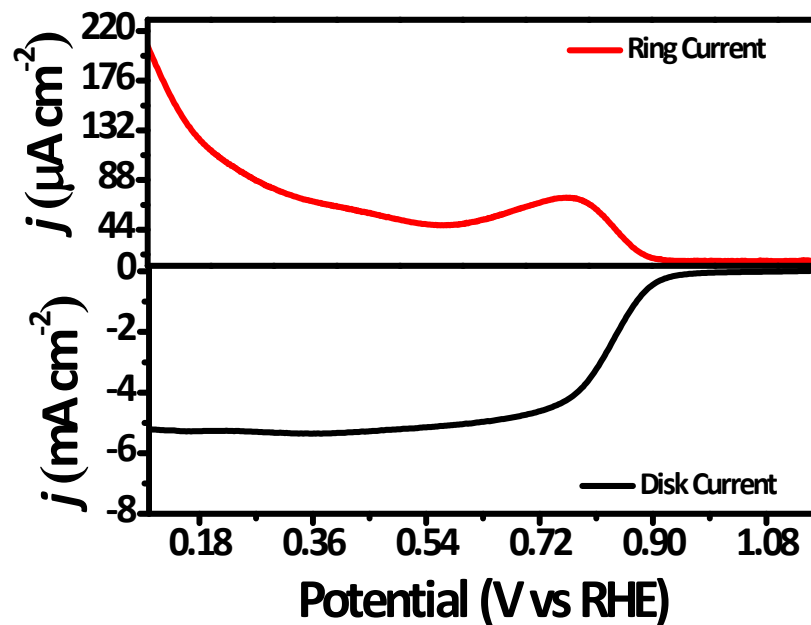


Fig. S17. Linear sweep voltammetry (LSV) polarization curve of FePP@G_{30/3/7} catalyst at 1600 rpm in O₂ saturated 0.1 M KOH electrolyte solution with disk and ring current.

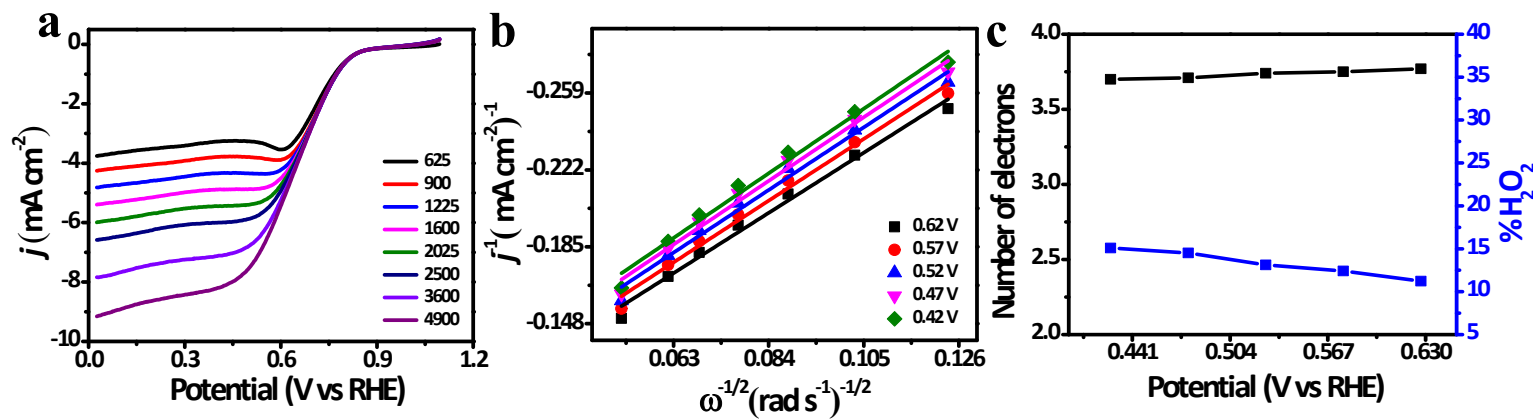


Fig. S18. (a) Linear sweep voltammetry (LSV) polarization curve of FePP catalyst all rotations from 625 to 4900 rpm (b) K-L Plots of FePP and (c) No. of electrons and %H₂O₂ of FePP catalyst in O₂ saturated 0.1 M KOH electrolyte solution.

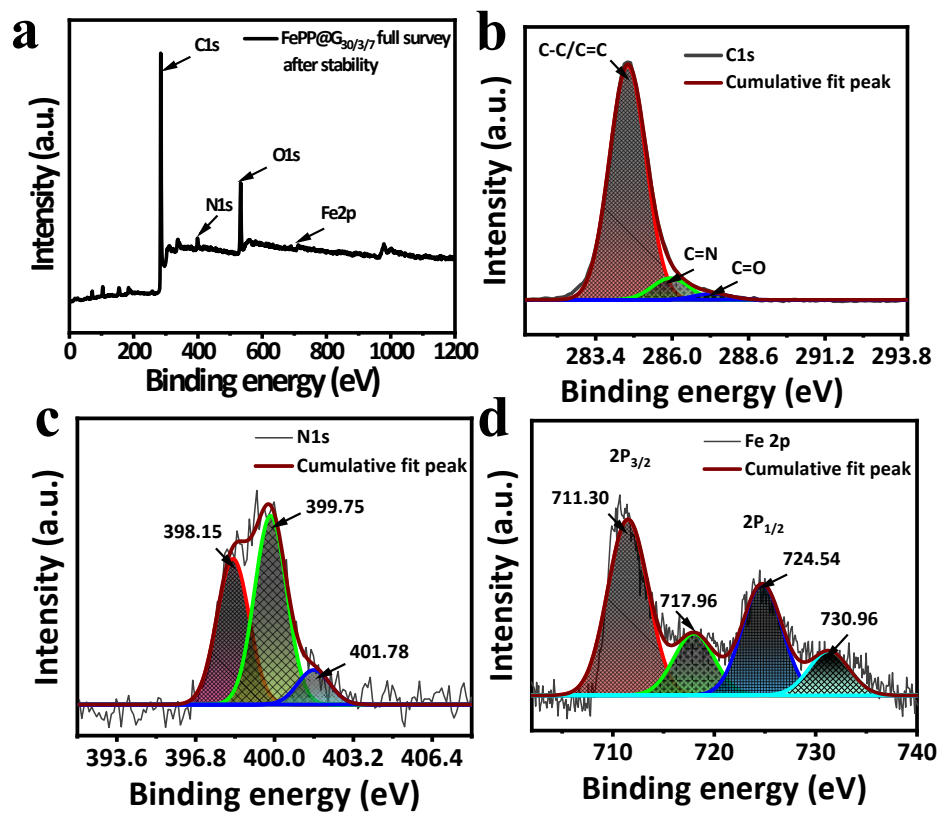


Fig. S19. XPS spectra of FePP@G_{30/3/7} catalyst after stability (a) Full survey XPS spectra. High resolution deconvoluted (b) C1s (c) N1s and (d) Fe2p XPS spectra of FePP@G_{30/3/7} catalyst after stability.

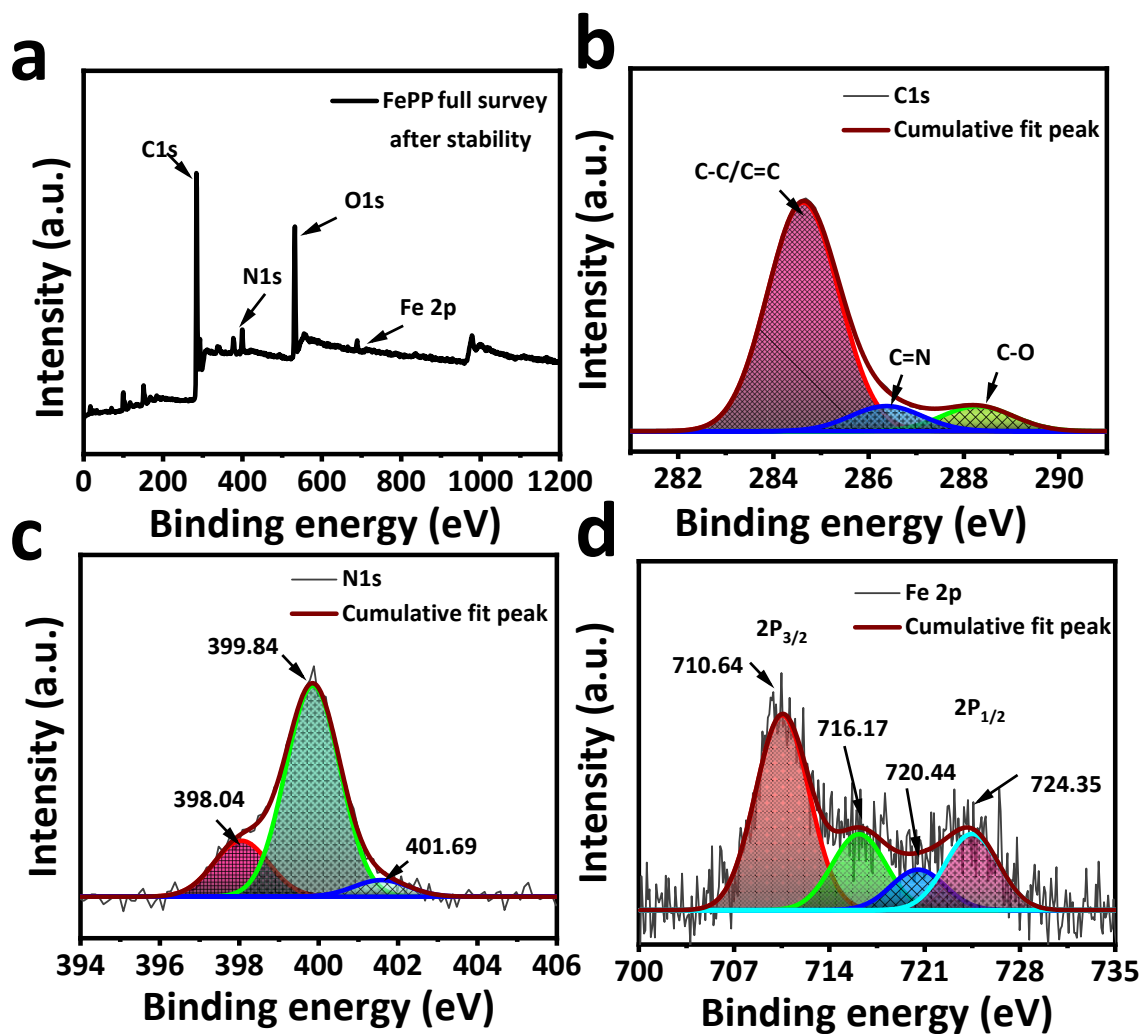


Fig. S20. XPS spectra of FePP catalyst after stability (a) Full survey XPS spectra. High resolution deconvoluted (b) C1s (c) N1s and (d) Fe2p XPS spectra of FePP catalyst after stability.

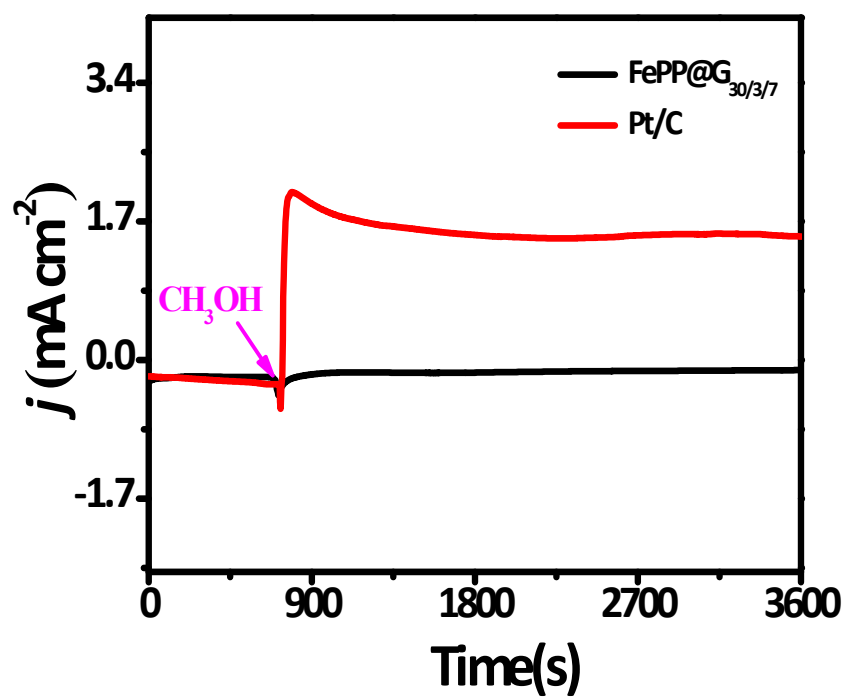


Fig. S21. Methanol cross over durability (i-t) curve in presence of methanol in O₂-saturated 0.1 M KOH solution.

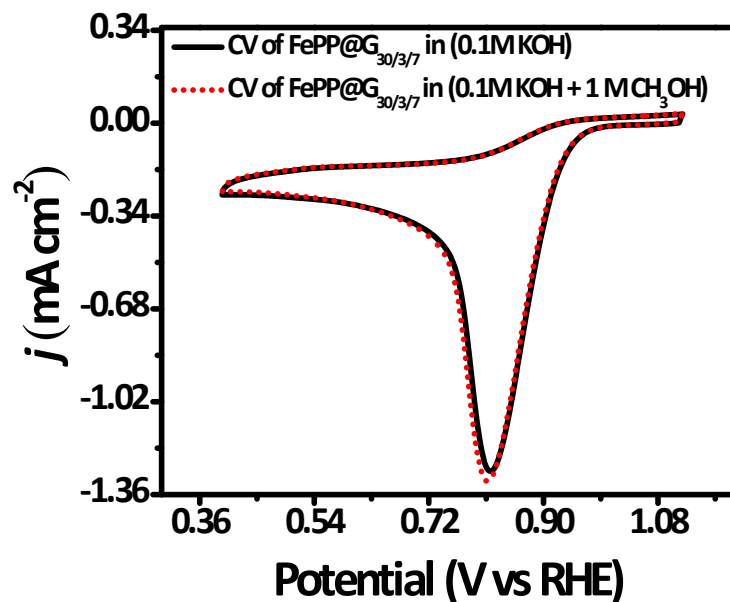


Fig. S22. CV analysis of FePP@G₃₀ catalyst with 1 M CH₃OH and without CH₃OH in O₂-saturated 0.1 M KOH electrolyte.

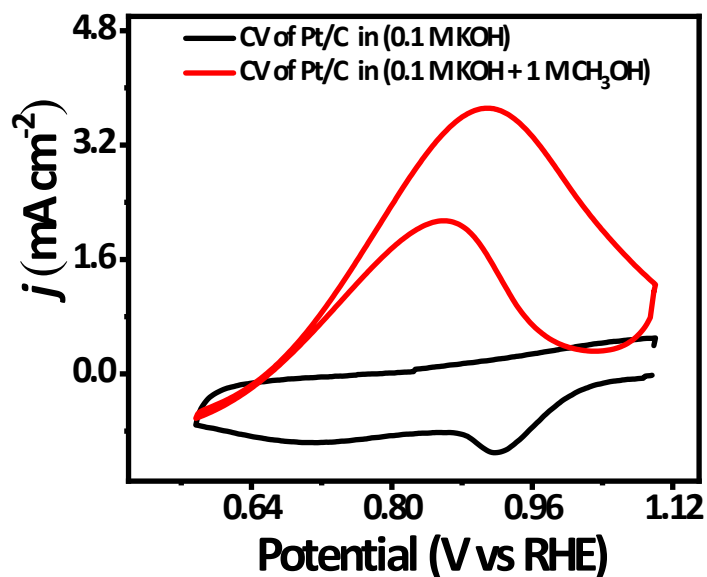


Fig. S23. CV analysis of Pt/C catalyst with 1 M CH₃OH and without CH₃OH in O₂-saturated 0.1 M KOH electrolyte.

In situ Raman analysis

In-situ Raman spectra were collected under controlled electrochemical potentials in O₂-saturated alkaline (0.1 M KOH) electrolyte using a three-electrode cell with a Ag/AgCl as a reference, Pt wire as a counter electrode and sample on copper foil as a working electrode. Raman spectroscopic data were collected using a Raman spectrometer (WITEC) by a 532 nm excitation laser. To avoid the electrolyte contact, a 50x long working distance objective was used for focusing on the sample surface. Acquisition time was set as 10 s for the spectral Raman shift ranging from 500 to 2000 cm⁻¹ window using the grating.

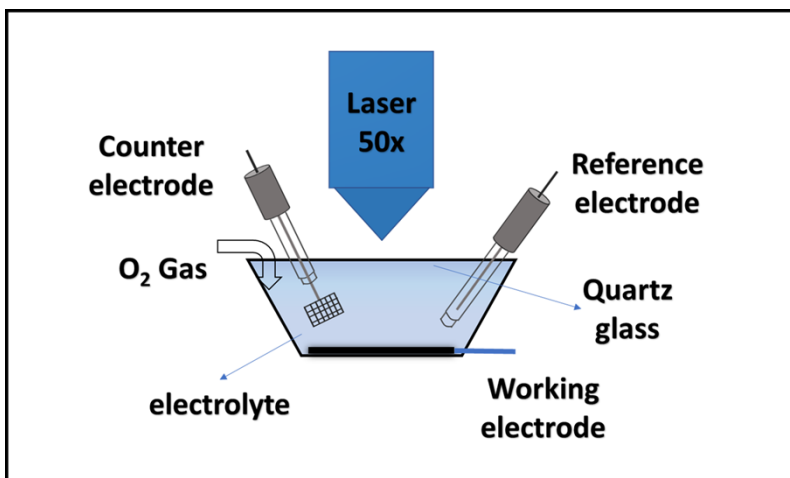


Fig. S24. Schematic for in-situ Raman setup during ORR analysis performed in 0.1 M KOH solution

In situ attenuated total reflection Fourier transformed infra-red (ATR-FTIR) spectroscopy

In situ electrochemical FT-IR spectroscopic studies were performed using a purged Bruker FT-IR spectrometer equipped with the Pike electrochemical cell accessory. A CaF_2 hemispherical crystal window was used with the working electrode placed 1 mm above the window for this in-situ FTIR study for ORR. The measurement parameters were 4 cm^{-1} resolutions and 64 scans. This setup enabled the recognition of ORR intermediate formation and change of adsorption of various intermediates within the thin-layer electrolyte on the electrode surface.

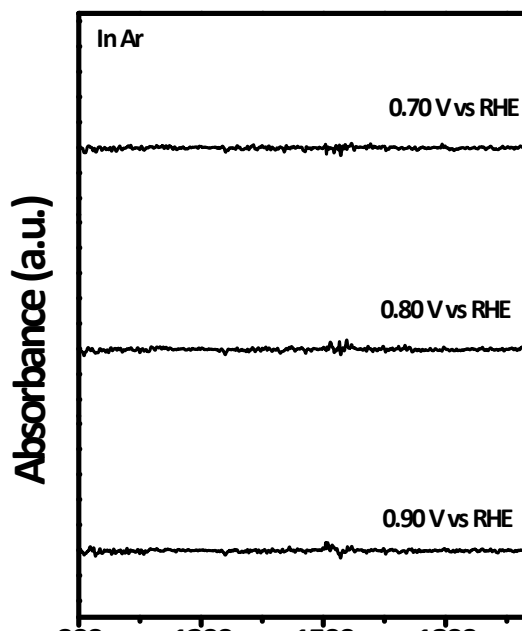


Fig. S25. In-situ FTIR spectra during ORR analysis in Ar-saturated 0.1 M KOH solution

Section-3

Theoretical Calculations

d-band center is calculated using formula

$$\frac{\int_{-\infty}^0 \rho_d E dE}{\int_{-\infty}^0 \rho_d dE}$$

Here ρ denote the density of d-band and E denotes the energy eigen value.

Free energy difference ΔG is calculated by,

$$\Delta G = \Delta E_{\text{DFT}} + \Delta \text{ZPE} - T\Delta S - neU$$

* represents active site on surface, molecules with * indicate adsorbed state. E_{DFT} , ZPE, TS, n and U represents total energy obtained through DFT calculation, zero-point energy of free molecules, entropy obtained through vibrational frequency calculations, number of electrons transferred and the applied potential at the electrode.

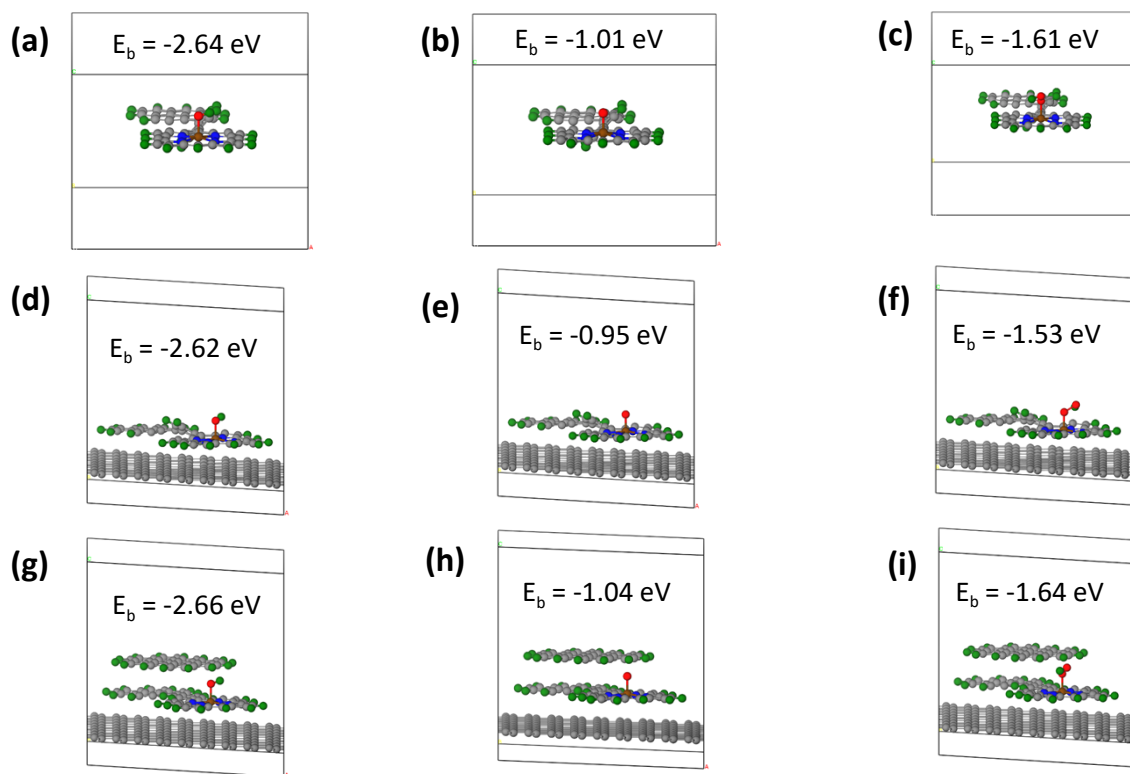


Fig. S26. Structure models of intermediates adsorbed on the surfaces. (a) OH on FePP (b) O on FePP (c) OOH on FePP, (d) OH on FePP/G (Ph ring out of plane) (e) O on FePP/G (Ph ring out of plane) (f) OOH on FePP/G (Ph ring out of plane) (g) OH on FePP@G_{30/3/7} (h) O on FePP@G_{30/3/7} (i) OOH on FePP@G_{30/3/7}.

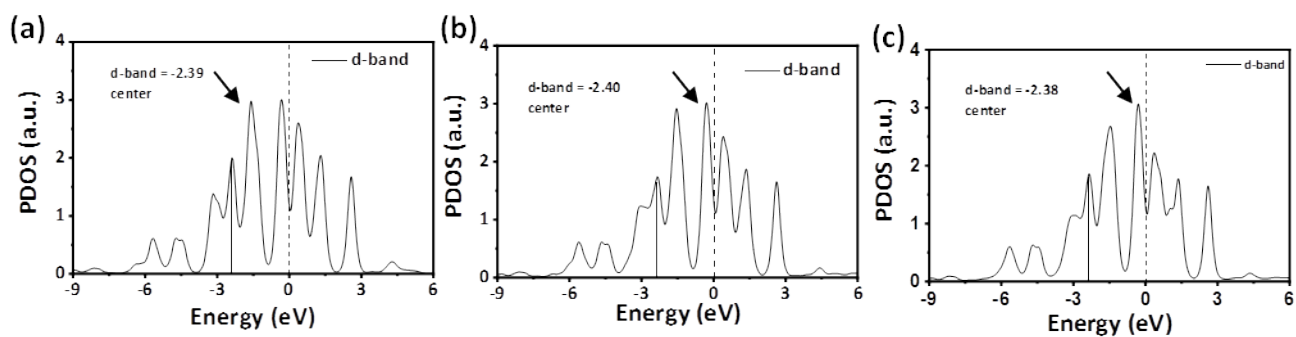


Fig. S27. Projected density of states (PDOS) of the d-orbital of (a) FePP, (b) FePP on single graphene sheet (Ph-ring out of plane) and (c) FePP between fixed graphene sheet and flake (FePP@G_{30/3/7}). Dashed vertical line represents Fermi level (E_F) and solid vertical line represents d-band center position. *Note: Up and down spin d-states are added to calculate the d-band center.*

Table 1. Raman spectroscopy analysis of all synthesized of FePP and FePP@G_{30/3/7} and EG catalysts

S. No	Sample	D-band (cm⁻¹)	G-band (cm⁻¹)	I_D/I_G ratio
1	FePP@G _{30/3/7}	1341	1574	0.87
2	FePP	1336	1574	0.93
3	EG	1340	1573	0.89

Table T2. Elemental analysis of FePP@G_{30/3/7} obtained from XPS analysis before and after stability.

S No.	Elements	FePP@G _{30/3/7} Catalyst			FePP Catalyst		
		Binding Energy (eV)	Atomic (%)		Binding Energy (eV)	Atomic (%)	
			Before stability	After stability		Before stability	After stability
1.	Carbon (C)	284.31	89.23	88.85	284.93	86.09	79.38
2.	Oxygen (O)	532.29	7.52	8.47	532.10	8.99	16.51
3.	Nitrogen (N)	398.94	2.77	2.23	399.35	3.87	3.61
4.	Iron (Fe)	711.17	0.48	0.45	711.83	1.05	0.51

Table T3. Different parameters obtained from the EXAFS fitting of FePP and FePP@G_{30/3/7} catalysts

Catalysts	Path	Coordination Number (N)	Bond length R (Å)	Bond disorder σ^2 (*10⁻³ Å²)	$\Delta E0$ (eV)	R-factor
FePP@G_{30/3/7}	Fe-N	4.088	1.98	2.77	1.24	0.02
FePP	Fe-N	3.99	2.03	5.80	2.75	0.03

Table T4. All the synthesized catalysts performances on the basis of electrocatalytic parameters

S. No.	Catalyst	Onset potential E_{onset} (V)	Half-wave potential $E_{1/2}$ (V)	Limiting current density J_L (mA cm⁻²)	Tafel slope (mV dec⁻¹)
1	FePP@G _{30/3/7}	0.947	0.84	5.27	72
2	FePP	0.866	0.71	5.22	92
5	FePP/G	0.869	0.701	3.09	106
6	FeP	0.701	0.67	1.41	111
7	Pt/C	0.997	0.86	5.43	77

Table T5. All the optimized exfoliated catalysts performances on the basis of electrocatalytic parameters

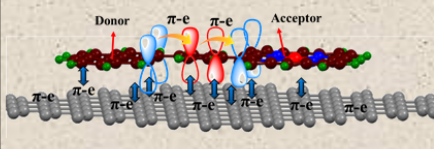
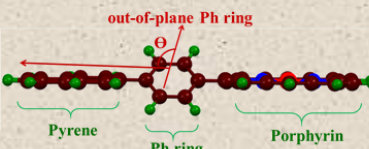
S. No.	Catalyst	Onset potential E_{onset} (V vs RHE)	Half-wave potential $E_{1/2}$ (V vs RHE)	Limiting current density J_L (mA cm⁻²)
1	FePP@G _{30/3/7}	0.947	0.84	5.27
2	FePP@G _{20/3/7}	0.886	0.75	4.66
3	FePP@G _{40/3/7}	0.929	0.83	5.13
4	FePP@G _{30/1.5/7}	0.863	0.73	4.01
5	FePP@G _{30/5/7}	0.910	0.77	3.85
6	FePP@G _{30/3/5}	0.859	0.79	3.91
7	FePP@G _{30/3/10}	0.895	0.76	4.85
8	FePP_SuperP	0.858	0.72	5.50
9	FePP_XC72	0.850	0.74	5.21

Table T6. Literature comparison of ORR performances with Fe-porphyrin based catalysts, Fe oxides and metal nanoparticles-based catalyst in alkaline electrolytes.

S. No	catalyst	Electrolyte	Onset potential	Half wave potential	Limiting current density	Reference
1	FePP@G_{30/3/7}	0.1 M KOH	0.947 V vs RHE	0.84 V vs RHE	5.27 mA cm⁻²	This work
2	(FeP)n-CNTs	0.1 M KOH	0.88 V vs RHE	0.76 V vs RHE	4.5 mA cm ⁻²	8
3	Fe-porphyrin-1/CNT	0.1 M KOH	0.930 V vs RHE	0.84 V vs RHE	5 mA cm ⁻²	9
4	FeTPPCL/C catalyst	0.1M NaOH	0.95 V vs RHE	-	4.5 mA cm ⁻²	10
5	Fe(III)TMPyP	0.1 M TFMSA	-	-0.128 V vs RHE	5.3 mA cm ⁻²	11
6	HT800-FeP	0.1 M KOH	0.96 V vs RHE	0.86 V vs RHE	4 mA cm ⁻²	12
7	FeTMPPCL-XC72	0.1 M HClO ₄	-	0.34 V vs RHE	5 mA cm ⁻²	13
8	Fe-DOH/C	0.5 M H ₂ SO ₄	0.73 V vs RHE	0.45 V vs RHE	4.8 mA cm ⁻²	14
9	MWCNTs-Im-FeF ₂₀ TPP	0.1 M KOH	1.04	0.87 V vs RHE	5 mA cm ⁻²	15
10	C@PVI-(DFTPP)Fe-800	0.1 M KOH	0.99 V vs RHE	0.88 V vs RHE	7 mA cm ⁻²	16
11	Fe ₇ -Ce ₁ @GSL-800	0.1 M KOH	0.977 V vs RHE	0.87 V vs RHE	-	17
12	FNCO-01	0.1 M KOH	0.825 V vs RHE	-	3.6 mA cm ⁻²	18
13	Fe _x N _y /NC	0.1 M KOH	-	0.77 V vs RHE	6 mA cm ⁻²	19
14	Fe-MFC ₆₀ -150	0.5 M KOH	0.85 V vs RHE	0.78 V vs RHE	2.9 mA cm ⁻²	20
15	FeS/G(Fe/GO=1:4)	0.1 M KOH	1.0 V vs RHE	0.845 V vs RHE	-	21

)					
16	Cu/Fe@ γ - Fe ₂ O ₃ @C	0.1 M KOH	0.86 V vs RHE	0.69 V vs RHE	5.1 mA cm ⁻²	22
17	Fe/P/C _{0.5} -800	0.1 M KOH	0.884 V vs RHE	0.815 V vs RHE	-	23
18	Fe ₃ C/C-800	0.1 M KOH	1.05 V vs RHE	0.83 V vs RHE	3.9 mA cm ⁻²	24
19	Fe _x P/NPCS	0.1 M KOH	0.918 V vs RHE	0.832 V vs RHE	5.4 mA cm ⁻²	25
20	α -Fe ₂ O ₃ /CNTs	0.1 M KOH	-0.15 V vs Ag/AgCl	-	3.89 mA cm ⁻²	26
21	FeCoNi-CNTs-2	1.0 M KOH	0.96 V vs RHE	0.82 V vs RHE	7.1 mA cm ⁻²	27
22	FeCo ₂ O ₄ -M	0.1 M KOH	0.91 V vs RHE	0.80 V vs RHE	4.68 mA cm ⁻²	28

Table T7. Comparative summary of all the electronic as well as electrochemical parameters of FePP@G_{30/3/7} and FePP catalysts

Feature	FePP@G _{30/3/7}	FePP
Ph-ring flipping		
Evidence		
UV spectra – π - π^* transition	330 nm (red shift), enhanced π -conjugation between FePP moiety and graphene	307 nm
Solid-state photoluminescence (ss-PL)	High intense peak at 395 nm	Very less intense peak at 395 nm
Raman	$I_D/I_G = 0.87$	$I_D/I_G = 0.93$
Consequence		
Resistivity	28.9017 Ω (ten-fold decrease), enhanced π -electron flow throughout the system	1.976 X10 ⁷ Ω
Work function	4.34	5.77
ORR performance		
Half wave potential ($E_{1/2}$)	0.84 V	0.71 V
ORR overpotential	0.64 V	0.72V

References

- 1 S. K. Das, S. Shyamal, M. Das, S. Mondal, A. Chowdhury, D. Chakraborty, R. S. Dey and A. Bhaumik, *Front Chem*, 2021, **9**, 1094.
- 2 G. Kresse and J. Furthmüller, *Comput Mater Sci*, 1996, **6**, 15–50.
- 3 P. E. Blöchl, *Phys Rev B*, 1994, **50**, 17953.
- 4 J. P. Perdew, K. Burke and M. Ernzerhof, *Phys Rev Lett*, 1996, **77**, 3865.
- 5 S. Grimme, *J Comput Chem*, 2006, **27**, 1787–1799.
- 6 W. Tang, E. Sanville and G. Henkelman, *Journal of Physics: Condensed Matter*, 2009, **21**, 084204.
- 7 A. Baby, D. Singh, C. Murugesan and P. Barpanda, *Chemical Communications*, 2020, **56**, 8400–8403.
- 8 H. Jia, Z. Sun, D. Jiang, S. Yang and P. Du, *Inorg Chem Front*, 2016, **3**, 821–827.
- 9 L. Xie, X. P. Zhang, B. Zhao, P. Li, J. Qi, X. Guo, B. Wang, H. Lei, W. Zhang, U. P. Apfel and R. Cao, *Angew Chem Int Ed Engl*, 2021, **60**, 7576–7581.
- 10 N. Ramaswamy and S. Mukerjee, *Advances in Physical Chemistry*, , DOI:10.1155/2012/491604.
- 11 Q. He, T. Mugadza, X. Kang, X. Zhu, S. Chen, J. Kerr and T. Nyokong, *J Power Sources*, 2012, **216**, 67–75.
- 12 N. Zion, J. C. Douglin, D. A. Cullen, P. Zelenay, D. R. Dekel, L. Elbaz, N. Zion, L. Elbaz, J. C. Douglin, D. R. Dekel, D. A. Cullen and P. Zelenay, *Adv Funct Mater*, 2021, **31**, 2100963.
- 13 Q. Hua, K. E. Madsen, A. M. Esposito, X. Chen, T. J. Woods, R. T. Haasch, S. Xiang, A. I. Frenkel, T. T. Fister and A. A. Gewirth, *ACS Catal*, 2022, **12**, 1139–1149.
- 14 G. Tei, T. Tamaki, T. Hayashi, K. Nakajima, A. Sakai, S. Yotsuhashi and T. Ogawa, *Eur J Inorg Chem*, 2017, **2017**, 3229–3232.
- 15 X. Y. Zhou, C. Xu, P. P. Guo, W. L. Sun, P. J. Wei and J. G. Liu, *Chemistry – A European Journal*, 2021, **27**, 9898–9904.
- 16 Y.-M. Zhao, P.-C. Zhang, C. Xu, X.-Y. Zhou, L.-M. Liao, P.-J. Wei, E. Liu, H. Chen, Q. He and J.-G. Liu, *ACS Appl Mater Interfaces*, 2020, **12**, 17334–17342.
- 17 J. Long, C. Chen and X. Gou, *J Colloid Interface Sci*, 2022, **625**, 555–564.
- 18 Y. T. Lu, Y. J. Chien, C. F. Liu, T. H. You and C. C. Hu, *J Mater Chem A Mater*, 2017, **5**, 21016–21026.
- 19 M. J. Park, J. H. Lee, K. P. S. S. Hembram, K. R. Lee, S. S. Han, C. W. Yoon, S. W. Nam and J. Y. Kim, *Catalysts*, , DOI:10.3390/catal6060086.

- 20 M. R. Benzigar, S. Joseph, G. Saianand, A. I. Gopalan, S. Sarkar, S. Srinivasan, D. H. Park, S. Kim, S. N. Talapaneni, K. Ramadass and A. Vinu, *Microporous and Mesoporous Materials*, 2019, **285**, 21–31.
- 21 J. Gautam, D. T. Tran, T. I. Singh, N. H. Kim and J. H. Lee, *J Power Sources*, 2019, **427**, 91–100.
- 22 M. Wang, C. Su, M. Saunders, J. Liang, Z. Shao, S. Wang and J. Liu, *Particle and Particle Systems Characterization*, , DOI:10.1002/ppsc.201700158.
- 23 M. Li, T. Liu, X. Bo, M. Zhou, L. Guo and S. Guo, *Nano Energy*, 2017, **33**, 221–228.
- 24 Y. Hu, J. O. Jensen, W. Zhang, L. N. Cleemann, W. Xing, N. J. Bjerrum and Q. Li, *Angewandte Chemie - International Edition*, 2014, **53**, 3675–3679.
- 25 K. Hu, Z. Xiao, Y. Cheng, D. Yan, R. Chen, J. Huo and S. Wang, *Electrochim Acta*, 2017, **254**, 280–286.
- 26 M. Sun, Y. Dong, G. Zhang, J. Qu and J. Li, *J Mater Chem A Mater*, 2014, **2**, 13635–13640.
- 27 H. Fang, H. Bian, B. Hu, J. Liu, S. Li, M. H. Wang, L. He and Z. Zhang, *Appl Surf Sci*, , DOI:10.1016/j.apsusc.2022.154590.
- 28 Z. Zhang, J. Li, J. Qian, Z. Li, L. Jia, D. Gao and D. Xue, *Small*, , DOI:10.1002/smll.202104248.